Journal of Polymers and the Environment (2024) 32:3735–3748
https://doi.org/10.1007/s10924-024-03191-y

ORIGINAL PAPER

Recent Progress in Enhanced Optical, Mechanical, Thermal Properties, and Antibacterial Activity of the Chitosan/Polyvinylalcohol/Co_3O_4 Nanocomposites for Optoelectronics and Biological Applications

Hanan Alhussain[1] · Azzah M. Alghamdi[2] · Nuha Y. Elamin[1,3] · A. Rajeh[4]

Accepted: 10 January 2024 / Published online: 19 February 2024

Abstract

The present study explores the influence of Cobalt oxide nanoparticles(Co_3O_4 NPs) on the physicochemical characteristics of Poly(vinylalcohol)/ Chitosan (PVA/Cs) blend. Using a variety of techniques, the pure blend and the nanocomposites' composition, structure, optical, thermal, and mechanical properties, and antibacterial activity were characterized. The Co_3O_4 NPs were produced by precipitation method utilizing cobalt salt as the raw material. The crystalline nature of the nanoparticles and semi-crystalline behavior of the PVA/Cs are demonstrated by the XRD data. Adding nanoparticles to the pure blend reduced the intensity of the semi-crystalline. The rise in absorption intensity observed in UV-visible spectra upon the incorporation of Co_3O_4 NPs into the PVA/Cs blend indicates an improved dispersion of the nanoparticles within the blend. When Co_3O_4 NPs are added, the energy band-gap E_{gdir} and E_{gind} of PVA/Cs–Co_3O_4 samples greatly decrease. According to TGA data, the thermal stability of nanocomposites was significantly higher than that of the PVA/Cs blend, and it rose as the concentration of nanoparticles increased. When compared to neat PVA/Cs film, mechanical property investigation of PVA/Cs–Co_3O_4 nanocomposites films revealed enhanced features. The effectiveness of the PVA/Cs–Co_3O_4 nanocomposite films in inhibiting the growth of microorganisms was assessed by evaluating their antimicrobial activity (ANMAC) against a range of bacteria and fungi. The inclusion of Co_3O_4 NPs led to an increase in activity against Gram-positive *Staphylococcus aureus* (*S. aureus*) and Gram-negative *Escherichia coli* (*E. coli*) bacteria as well as fungi *Candida albicans* and *Aspergillus niger* (*C. albicans and A. niger*). The addition of Co_3O_4 NPs to the PVA/Cs blend effectively improved the material's optical, thermal, mechanical, and antibacterial properties. This remarkable improvement stems from the Co_3O_4 NPs, which were introduced into the PVA/Cs blend in different amounts, leading to the development of novel nanocomposites. The outstanding properties of Co_3O_4/PVA/Cs nanocomposite films suggest their potential for applications in optoelectronics and food packaging.

Keywords Co_3O_4 nanoparticles · Optical properties · Thermal properties · Mechanical properties · Antimicrobial activity

✉ Hanan Alhussain
hmalhussain@imamu.edu.sa

✉ Azzah M. Alghamdi
amalghamdi@uj.edu.sa

✉ A. Rajeh
a.rajeh88@yahoo.com

[1] Department of Chemistry, College of Science, Imam Mohammad Ibn Saud Islamic University (IMSIU), P.O. Box 5701, 11432 Riyadh, Saudi Arabia

[2] College of Science, Department of Physical Sciences, University of Jeddah, Jeddah, Saudi Arabia

[3] Department of Chemistry, Sudan University of Science and Technology, P.O. Box 407, 11111 Khartoum, Sudan

[4] Physics Department, Faculty of Applied Science, Amran University, Amran, Yemen

Introduction

The creation and processing of nanocomposite materials with a polymer matrix that possesses bio-safe attributes like biocompatibility and biodegradability may be of relevance in the current contaminated surroundings. Polymer nanocomposites (PNCs) have gained prominence in various scientific disciplines, including biology, electronics, and mechanics, due to their exceptional mechanical, biological, and physical properties [1]. Polymer nanocomposites (PNCs) offer significant advantages over polymers doped with micron-sized nanofillers, including enhanced thermo-mechanical properties such as degradation resistance and dielectric strength. The incorporation of suitable fillers can effectively tailor the mechanical, optical, thermal properties,

and antimicrobial activity (ANMAC) of polymers to meet specific requirements [2, 3]. One of the earth's most prevalent naturally occurring alkaline polysaccharides is chitosan (Cs) biopolymer [4]. The pursuit of innovative polymer electrolytes, biopolymers, or polysaccharides such as Cs, carboxymethyl cellulose, and cellulose, holds promise as host polymer networks [5, 6]. One of the many benefits of biopolymers, particularly Cs, is that they are inexpensive, readily available, and environmentally benign [7]. Additionally, they contain β (1–4)-linked D-glucosamine de-acetylated linear polysaccharide [8, 9]. Two atoms, O and N, in Cs, have a lone pair of electrons [8]. The backbone of Cs contains ether (C–O–C), O–H group, and amine (NH_2) that enable potential interactions between the cations of filler and other polymers like PVA, PVP, etc. in terms of polymer blending [10, 11]. PVA possesses a wealth of O-H group with its side chains, imparting excellent water solubility and tunable optical and electrical properties upon doping. Their properties make them a good choice for blending with Cs. PVA, a non-toxic, biocompatible, water-soluble, and biodegradable synthetic polymer, stands as a versatile host polymer for preparing polymer blends with biopolymers [12]. . The O–H groups along the side chains of polyvinyl alcohol facilitate interactions with other polymers and biopolymers containing functional groups like those in chitosan, enabling the formation of miscible polymer blends [8]. It's possible that using a single biopolymer won't provide good chemical, optical, or mechanical flexibility. Polymer blending emerges as a promising strategy to improve the mechanical flexibility, optical properties, and ionic conductivity, of electrolytes [13]. Nano-composite films based on Cs/PVA-ZnO exhibit antimicrobial activity [14]. The polymer network's semi-crystalline phase shows constrained segmental motion of the polymer chains as well as limited free space between and polymer chains the along. The physical properties of polymers are influenced by the nature of chemical of the nanofiller and its interactions with the polymer blend. The properties of polymer matrices can be significantly enhanced by incorporating various nanofillers, such as carbon nanotubes, metal oxides, and rare earth doped ions. The effectiveness of these nanofillers depends on their interaction and dispersion within the polymeric matrices [15]. Due to their special adjustable optical characteristics, bimetallic nanoparticles are utilized extensively [16]. In addition to the need for novel materials in optical and optoelectronic applications, the introduction of novel medications is critically needed because of infections spread by various bacteria [17]. The Co_3O_4, a versatile inorganic material, has found widespread applications in both bulk and nano forms across various fields, including electrochemical systems, electrochromic devices, water electrolysis processes, high-temperature solar selective absorbers, and rechargeable lithium-ion batteries [18, 19]. The potential formulation of a novel class of bactericidal materials may be made possible by the Co_3O_4 nanoparticles. Despite the growing interest in cobalt oxide nanoparticles, there is a dearth of research investigating their antibacterial potential. A limited number of recent investigations have demonstrated that Co_3O_4 NPs exhibit synergistic antibacterial effects and can combat both gram-negative and gram-positive bacteria [19, 20]. V. Gupta et al. [21] explored the antibacterial activity of Co_3O_4 NPs across a range of concentrations and compared their efficacy to established antibiotics tetracycline and gentamicin. The antibacterial efficacy of these nanoparticles demonstrated their potential to reduce the environmental burden of pathogenic bacteria and combat antibacterial resistance and could be applied in different areas like food packages, water disinfection, medical sciences, etc. This study focuses on the fabrication of Co_3O_4 NPs as nanofiller to investigate their impact on the physical and chemical properties of PVA/Cs blend. A comprehensive characterization of PVA/Cs blend has been conducted using various techniques to evaluate its structural, optical, thermal, mechanical, and antifungal properties. This extensive investigation will contribute to the development of novel nanocomposites with potential applications in antimicrobial packaging and optoelectronic devices.

Materials and methods

Materials

Polyvinyl alcohol (PVA) $(C_2H_4O)n$, 99% purity, and M.W = 14,000 g/mol purched from E-Merck, Germany. Chitosan powder (Cs) has a medium molecular weight, viscosity: 200–800 cP, and 75–85% deacetylated from Sigma-Aldrich. Deionized water (DW) was used as solvent.

Synthesis of Co_3O_4 Nanoparticles

Co_3O_4 NPs were prepared via the precipitation of cobalt salt in an alkaline medium [21]. In brief, a 3 M sodium hydroxide solution was used to raise the pH of an aqueous $CoCl_2$ solution (0.6 M) to 10.5 after it had been heated to 80 °C. After two hours of stirring the solution at 80 °C, the precipitates-green cobalt hydroxide were centrifuged and then washed with distilled water and ethanol until the pH became 7. After that, the precipitate was dried for 12 h and finally was annealed for three hours at 150 °C to produce powdered Co_3O_4 NPs.

Synthesis of PVA/Cs- Co_3O_4 Nanocomposite Films

To commence the process, 0.2 g powder of PVA was dissolved in 20 ml of DW by heating at 80 °C for four hours, followed by stirring until a transparent solution was

obtained. Concurrently, 0.8 g Cs powder was dissolved in a mixture of acetic acid and DW (2:8) by heating and stirring at 50 °C for four hours. Subsequently, both solutions were combined and stirred at RT for eight hours. To prepare the Co_3O_4 solution, Co_3O_4 nanoparticles were dispersed in 10 ml of DW using ultrasonication at room temperature for one hour. Subsequently, the desired amount of Co_3O_4 was added dropwise to the polymer mixture solution and stirred for approximately 12 h to achieve a homogeneous dispersion of Co_3O_4 nanoparticles in the PVA/Cs (20/80 wt%) matrix. Finally, the uniformly dispersed solution was poured into a glass Petri dish and cast at 50 °C for five days. The resulting smooth and flexible blend and blend/ Co_3O_4 nanocomposites films were carefully peeled off and stored at room temperature for further characterization.

Antibacterial and Antifungal Activities Assay

Gram-negative bacteria (*Escherichia coli*) and Gram-positive bacteria (*Staphylococcus aureus*) were used to assess the produced compounds' antimicrobial properties. Two fungi were used to assess the compounds' anti-fungal properties (*Aspergillus niger*, *Candida albicans*). After dissolving each chemical in DMSO, a separate solution with a concentration of 1 mg/ml was created. Whatman filter paper discs in the typical size of 5 cm were manufactured, cut, and autoclave-sanitized. The petri plates containing nutrient agar media (agar 20 g + beef extract 3 g + peptone 5 g) seeded with *S. aureus*, E. coli, *C. albicans*, and *A. niger* were aseptically filled with paper discs soaked in the necessary concentration of the complex solution. After 24 h of incubation at 36 °C, the inhibition zones in the petri dishes were measured. The test agent's antibacterial activity was assessed by measuring the zone of inhibition's diameter, which was expressed in millimeters (mm). Each treatment was replicated three times, and the average reading was reported [22]. Using the same protocol as previously described, the antifungal *Colitrimazole* and the common standard antibiotic *ampicillin* were also tested for antibacterial activity at the same concentrations and solvent combinations.

Characterization Techniques

Using Copper Kα radiation, X-ray diffraction (XRD) analysis was carried out using the Pan analytical X' Pert PRO XRD system at a wavelength of λ = 1.540 A°. Transmission electron microscopy (JEOL 1200 EX) was utilized to specify the shape and particle size distribution of Co_3O_4. The prepared films were analyzed at room temperature using FT-IR spectroscopy (Nicolet iS10, USA) in the 4000–500 cm^{-1} range to identify the functional groups. Using a JASCO 630 Japan ultraviolet–visible (UV–vis) spectrophotometer in the 190–800 nm wavelength range, optical properties were measured at room temperature. Thermogravimetric analysis (TGA) was carried out utilizing an STD-Q600 thermal analyzer (USA) at a heating rate of 10 °C min^{-1} in N_2. To examine the mechanical characteristics of the nanocomposite films, the AMETEK LLOYD (LLOYD-5 KN, London, UK) Universal Testing Machine (UTM) was utilized.

Results and Discussion

XRD

To explore the structural modifications induced by the incorporation of Co_3O_4 nanoparticles into the PVA/Cs polymer blend, X-ray diffraction (XRD) measurements were conducted. Figure 1a reveals the crystalline structure of the synthesized Co_3O_4 nanoparticles, as evidenced by the sharp peaks in the XRD pattern. The absence of any additional peaks confirms the purity of the nanoparticles, indicating the successful synthesis of Co_3O_4 nanoparticles without any impurities. The XRD pattern exhibits a prominent

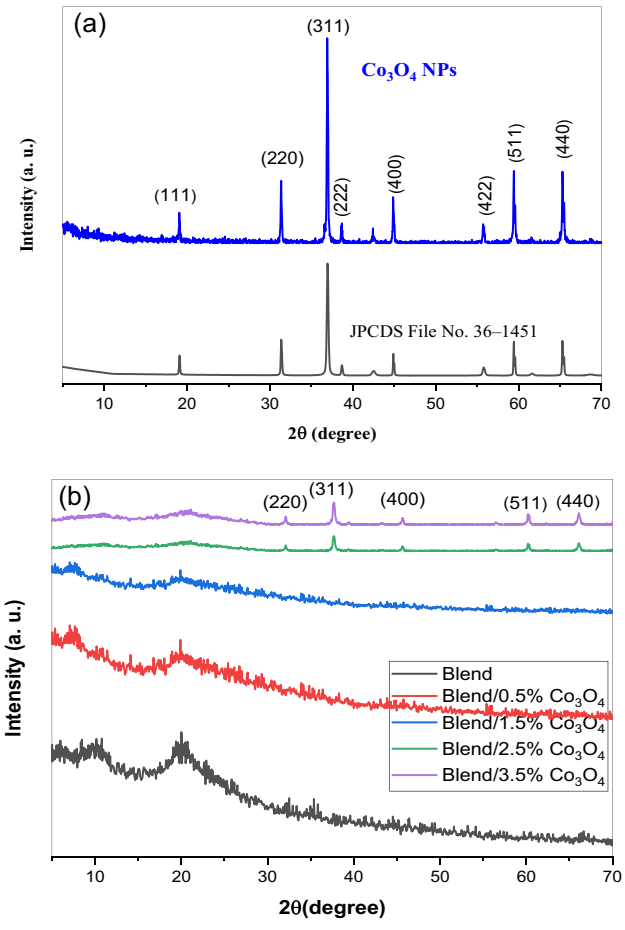

Fig. 1 XRD pattern of **a** Co_3O_4 nanoparticles and **b** pure blend and blend/x (wt%) Co_3O_4 nanocomposites films

peak at 37.65°, corresponding to the (311) plane of cobalt oxide crystals. Additional well-defined diffraction peaks are observed at 19.0°, 31.91°, 37.65°, 38.68°, 44.89°, 55.72°, 59.61° and 65.82° corresponding to the (111), (220), (311), (222), (400), (422), (511) and (440) planes, respectively with lattice constants for the Co_3O_4 phase of = 0.521 nm and = 0.324 nm, respectively (JPCDS File No. 36–1451) [23]. The formation of crystalline Co_3O_4 nanoparticles is confirmed by XRD. The Scherrer equation ($D = 0.9\lambda/\beta \cos\theta$) was used to determine the crystal sizes of Co_3O_4, the crystallite size is 12.5 nm [24]. The dislocation density is determined using the following equation [25]:

$$\delta = 1/D^2 \quad (1)$$

Through this equation, it is observed that the dislocation density value of the pure Co_3O_4 is 6.4×10^{-3} m^{-2}. Micro strain (ε) value of Co_3O_4 NPs can be calculated using the formula [26]:

$$\varepsilon = b/4\tan\theta \quad (2)$$

where, β is the full width at half maximum (FWHM). It was observed that the value of the Micro strain (ε) for pure Co_3O_4 using this equation was 1.62×10^{-3}.

Figure 1b illustrates the XRD patterns of PVA/Cs-based polymer blend samples incorporated with varying contents of Co_3O_4 NPs. The broad peak observed at $2\theta = 20.21°$ for the pure polymer blend film is attributed to its semi-crystalline nature, arising from intramolecular and intermolecular interactions between polymer chains through hydrogen bonding. The XRD peak exhibits broadening and a decrease in intensity upon the introduction of Co_3O_4 nanoparticles, implying a reduction in the crystallinity of the polymer nanocomposite films [27, 28]. The 1.5%Co_3O_4/PVA/Cs and 0.5%Co_3O_4/PVA/Cs samples do not exhibit any peaks in intensity for Co_3O_4 NPs, as can be seen from the XRD diffractogram, which suggests that the added nanoparticles have dissociated. The broadening of XRD peaks, indicative of increased amorphicity, likely contributes to the higher ionic density and enhanced ionic conductivity observed in this sample [29]. The incorporation of Co_3O_4 nanoparticles induced slight shifts in the XRD peaks compared to the pure polymer blend, suggesting effective interactions between the nanofiller and the polymer matrix. Notably, the 2.5% PVA/Cs and 3.5% PVA/Cs samples exhibit sharp crystalline peaks at diffraction angles of 31.91°, 37.65°, 38.68°, 44.89°, 55.72°, 59.61° and 65.82°, which can be ascribed to the recrystallization of Co_3O_4 nanoparticles on the film surface due to ion recombination at higher Co_3O_4 NPs concentrations and may be due to agglomeration/aggregation of Co_3O_4NPs in blend [30]. The distinct diffraction peaks observed in samples with higher Co_3O_4 nanoparticle concentrations are in good agreement with the XRD data of the Co_3O_4 NPs.

Morphology Analysis by TEM

Transmission electron microscopy (TEM) was used to investigate the structural characteristics of the synthesized Co_3O_4 NPs as shown if Fig. 2. The TEM image presented in Fig. 2a revealed that the synthesized product exhibits a uniform morphology characterized by approximately spherical nanoparticles with a narrow size distribution. The small dimensions and high surface energy of these nanoparticles lead to a tendency for aggregation, as observed in Fig. 2a. The particle size histogram derived from the TEM image using the using SmartTiff software, shown in Fig. 2b, further

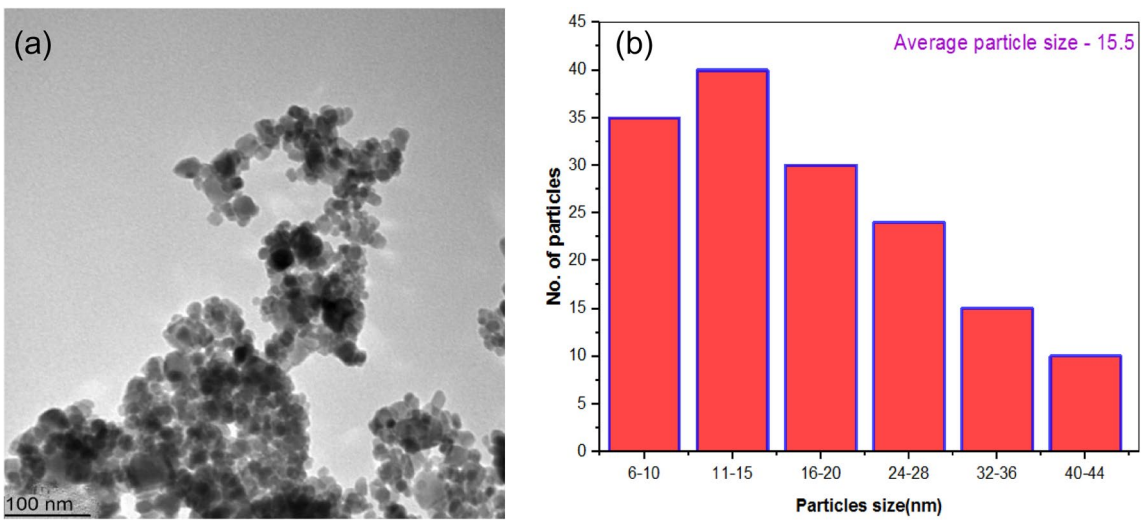

Fig. 2 **a** TEM image of the Co_3O_4 NPs and **b** Histogram showing the distribution of the Co_3O_4 nanoparticles size

confirms the narrow size distribution of the Co_3O_4 nanoparticles, with diameters predominantly ranging from 5 to 45 nm. The average particle size, determined to be 15.5 nm and a standard deviation of 5.23, is in close agreement with the value calculated using the Scherer equation based on the half-width of the diffraction peaks.

FTIR Spectra

Figure 3 presents the FTIR absorbance spectra of Pure Co_3O_4 NPs, pure Cs, pure PVA, pristine blend and blend/x(wt%) Co_3O_4 nanocomposites samples within the wavenumber range of 500 to 4000 cm^{-1}. The Co_3O_4's FTIR transmittance spectra were captured within a range of 4000 cm^{-1}–500 cm^{-1} as shown in Fig. 3a. The intensity of absorption linked to O–H groups and free water in the range of 3350 cm^{-1} to 3650 cm^{-1} is directly correlated with the moisture content of Co_3O_4. The bands ranging from 1370 cm^{-1} to 1596 cm^{-1} are indicative of carbonyls (C=O) and a strong three-bond alkyne group (C–C). The peaks 860 cm^{-1}, 696 cm^{-1}, and 620 cm^{-1} in the fingerprint region show that the sample contains a significant amount of ethers, esters, and carboxylic acids (C–C and C–O bonds) [31]. Figure 3b displays the infrared spectrum of pure Cs. For Cs, the axial stretching of the overlapped O–H and N–H bands is represented by the wide band in the 3100–3600 cm^{-1} range. Small bands at 2930 cm^{-1} and 2855 cm^{-1} are attributed to C–H in both $–CH_2$ and $–CH_3$ bonding, respectively. The typical absorption bands at 1654 cm^{-1} (amide I), 1588 cm^{-1} (amide II), and 1422, 1380 cm^{-1} (–CH, $–CH_2$ bending) [32] are visible in the chitosan spectrum Fig. 3b. The asymmetric vibrations stretching C–O in oxygen are responsible for the band at 1170 cm^{-1}, while the C–O of the ring COH and COC bonds are related to the bands at 1090 cm^{-1} [33]. The peaks at 3445 cm^{-1} and 1360 cm^{-1} for pure PVA were attributed to the PVA film's OH stretching and bending vibrations. At 2930 cm^{-1}, the peak corresponding to the asymmetric stretching vibration of the CH_2 was observed [34]. The unhydrolyzed ester functional group on the PVA backbone had a C=O, which was represented by the peak at 1670 cm^{-1}. The C–O–C asymmetric stretching vibration of the ester group could be responsible for the peak at 1270 cm^{-1} [35]. With a few exceptions to the PVA/Cs blend film's distinctive form and absorption band shifts brought about by hydrogen bonding between functional groups, the PVA/Cs blend film's spectra generally showed the same peaks as those seen in the Cs and PVA films. Therefore, in the studied blend, both intramolecular and intermolecular interactions are possible [36]. The FTIR spectrum of PVA/Cs blend exhibits characteristic bands at 3354 cm^{-1} and 3293 cm^{-1}, corresponding to the OH and N–H groups stretching vibrations, respectively. C–H symmetric and asymmetric stretching vibrations are attributed to the bands at 3304 cm^{-1}, 2921 cm^{-1}, and 2854 cm^{-1}, respectively. Additionally, peaks assigned to O=C–NHR stretching vibrations of the C=O and vibrations associated with amino group (N–H) appear at 1645 $cm^{-1}$and 1560 cm^{-1}, respectively. Bands at 1430 $cm^{-1}$and 1374 $cm^{-1}$are attributed to C–H bending and C–H wagging vibrations. The C–H wagging vibration band of the acetate residue is observed at 1243 cm^{-1}, and C–O stretching vibration bands are evident at 1088 cm^{-1} and 1021 cm^{-1} [14]. The FTIR spectra of blend/Co_3O_4 nanocomposites with varying Co_3O_4 nanoparticle loadings reveal characteristic peaks similar to those of the pure blend, as shown in Fig. 3c. The O–H bands and C–H symmetric and asymmetric bands shift towards lower wavenumbers upon Co_3O_4 nanoparticle incorporation. The peaks corresponding to O=C–NHR stretching and N–H bonding shift to lower wavenumbers, and the peaks at 1645 $cm^{-1}$and 1560 cm^{-1} become more intense with increasing nanoparticles loading [37, 38]. Similarly, the peak associated with C–N bending vibrations of Cs and C–OH stretching of PVA shifts to a lower wavenumber at 1090 cm^{-1}, while its intensity decreases significantly, indicating a reduction in the crystallinity of the pure blend [39]. The peak corresponding to the PVA skeletal vibration and the Cs saccharide structure exhibited a shift towards a lower wavenumber and a decrease in intensity upon nanofiller loading, indicating complexation between the functional groups of the nanofiller and the polymer blend (Scheme 1). This demonstrates that Co_3O_4 NPs and the polymeric chains are compatible.

UV–Vis Absorption

Ultraviolet-visible (UV–Vis) spectroscopy is a valuable tool for optical characterization. Figure 4 presents the absorption spectra of the pure PVA, Cs, pure blend and the blend doped with Co_3O_4 nanoparticles. A prominent shoulder band at 240 nm is monitored, which can be ascribed to the semi-crystalline nature of the pure blend and the presence of a C=O-containing structure associated with the polymer blend [40, 41]. These bands are ascribed to electronic transitions within the polymer backbone π–π* [14, 42]. The intensity of the absorption band increases with growing Co_3O_4 wt% in blend. These findings indicate an interaction between blend and nanofiller. Notably, none of the examined samples exhibited absorption bands in the visible region, confirming their transparency. This figure shows that, for all films, the absorption is roughly unchanged in the spectral range from 400 to 800 nm, but there is a significant change in the ultraviolet from 200 to 400 nm, where the fundamental absorption edge of the blend sample shifts towards a longer wavelength (red shift) in the blend-x wt.%Co_3O_4 ions nanocomposite samples and this shift increase by growing Co_3O_4

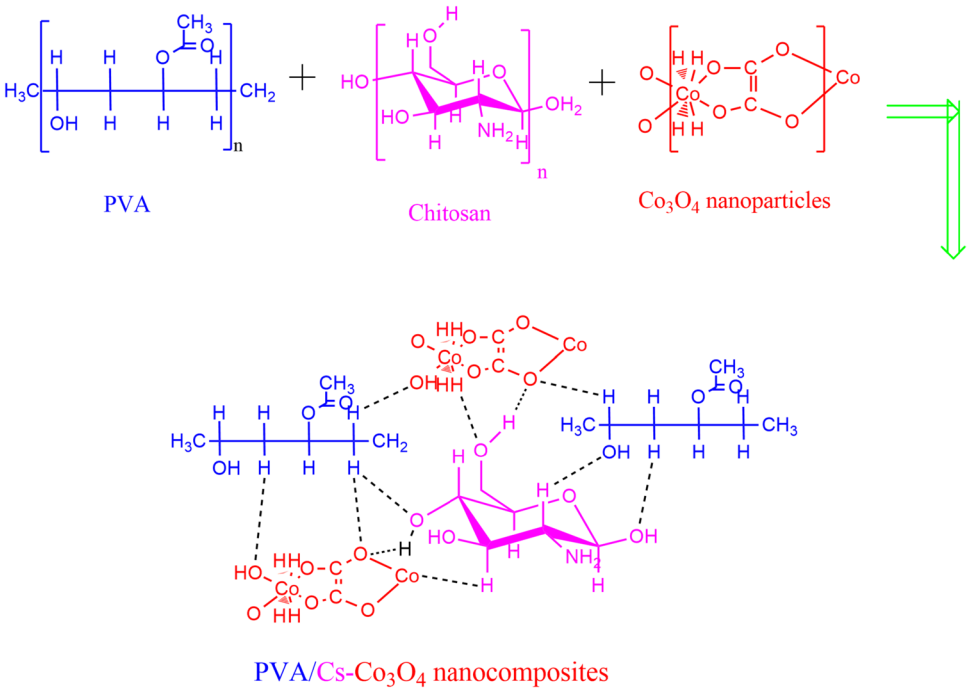

Scheme 1 The possible mechanism for interaction between PVA/Cs and PVA/Cs/Co_3O_4 NPs.

ions content in the blend demonstrates the complexation between blend and Co_3O_4 NPs which leads to in crystallinity change [43]. The absence of a well-defined optical absorption edge suggests a low degree of crystallinity in the films. Moreover, the absorbance edge is a defining characteristic of the charge transfer complex (CTC) formation between polymer blend chains and dispersed Co_3O_4 NPs [44, 45]. This result validates the highly wavelength-controllable absorbance behavior of this PNCs material, suggesting that it might be a good option for developing flexible devices that use spectral shorting in the future.

Determination of Optical band gap(OBG)

The OBG is a crucial method for defining the optical transition in prepared samples, as illustrated by Tauc's plot [46, 47].

$$(\alpha hn)^n = A\,(h\nu - E_g) \tag{3}$$

where *A* is a constant and the value n indicates the type of optical transformation; $n = 2$ and 1/2, respectively. Consistent with the findings of Hezma et al. [14], Fig. 5; Table 1 reveal an energy gap (direct and indirect) of 5.52 and 5.07 eV for PVA/Cs film. Nevertheless, the direct energy gap was reduced from 5.52 to 4.01 eV and the indirect energy gap was reduced from 5.07 to 3.56 eV by Co_3O_4 doping with a concentration ratio of 0.0wt.% and 2.5wt.% of PVA/Cs. This reduce in the optical bandgap can be explained by the formation of Co_3O_4 in the electronic structure of the PVA/Cs matrix, which is in charge of creating localized states between the band valence and conduction. Soliman et al. observed a decrease in the OBG as the $BaTiO_3$ concentration in the PVA matrix increased. This reduction is attributed to the introduction of defects that disrupt the orderliness of the polymer matrix [48]. Table 1 show that the E_{dir} and E_{ind} values gradually increase with the addition of only 3.5 wt% of Co_3O_4 to the PVA/Cs bend. The increase in polymer backbone conjugation and electron-donor nature, along with the addition of Co_3O_4, which splits the valence and conduction bands, are the reasons for this increase in the optical energy gap [49]. For the Co_3O_4NPs, there are two optical band gaps as shown in Fig. 5c, indicating direct allowed transitions. According to the figure, $\Delta Eg = 0.27$ eV separates the first band gap (E_{g1}), which is 1.52 eV, and the second band gap (E_{g2}), which is 1.79 eV. Additionally, very similar results for thin films and Co_3O_4NPs were found [50]. While $_{Eg1}$ is linked to the beginning of $O^{-2} \rightarrow Co^{+3}$ excitations, E_{g2} is attributed to the interband transition and is considered the basic or genuine band gap energy. The measured E_{g1} and $_{Eg2}$ are less than the bulk values of 2.85 eV and 1.70 eV, respectively. The quantum confinement effects in the nanomaterials could be the cause of this [51].

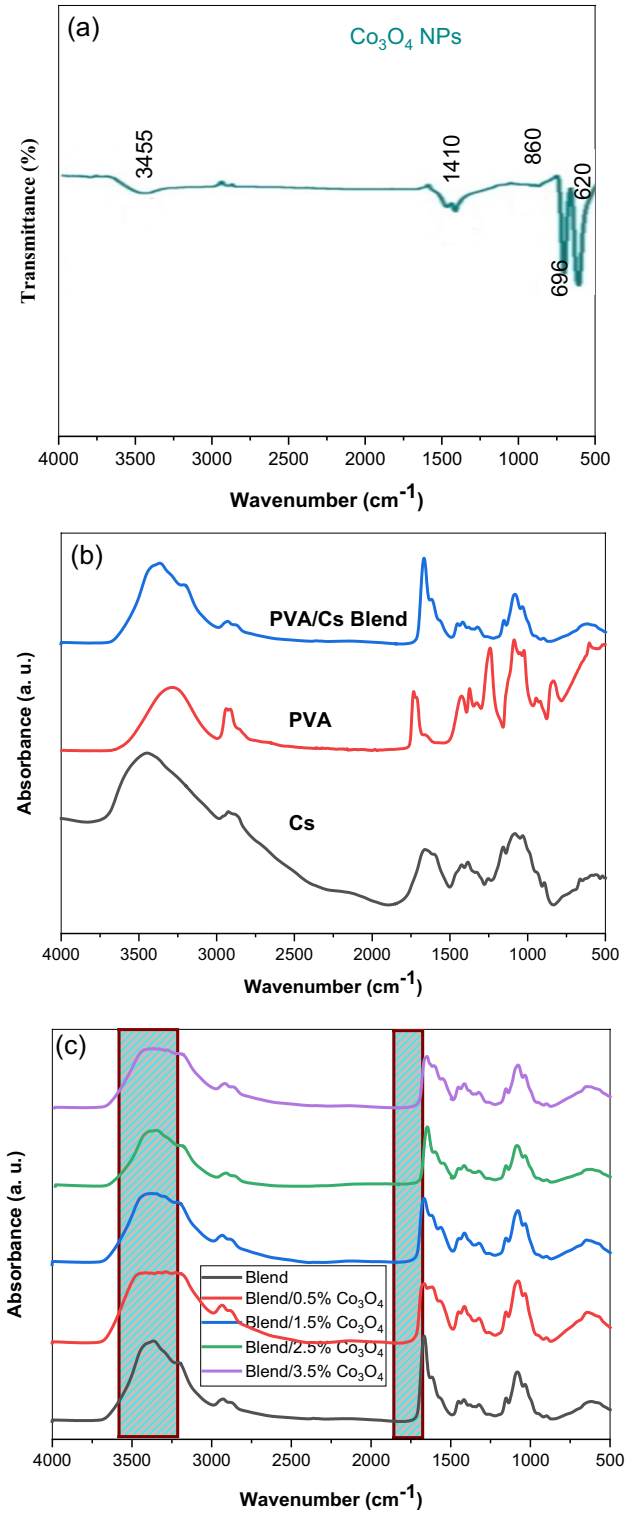

Fig. 3 FTIR absorbance spectra of **a** pure Co_3O_4 NPs, **b** pure Cs, pure PVA, and PVA/Cs blend **c** pure blend and PVA/Cs/x(wt%) Co_3O_4 nanocomposites films

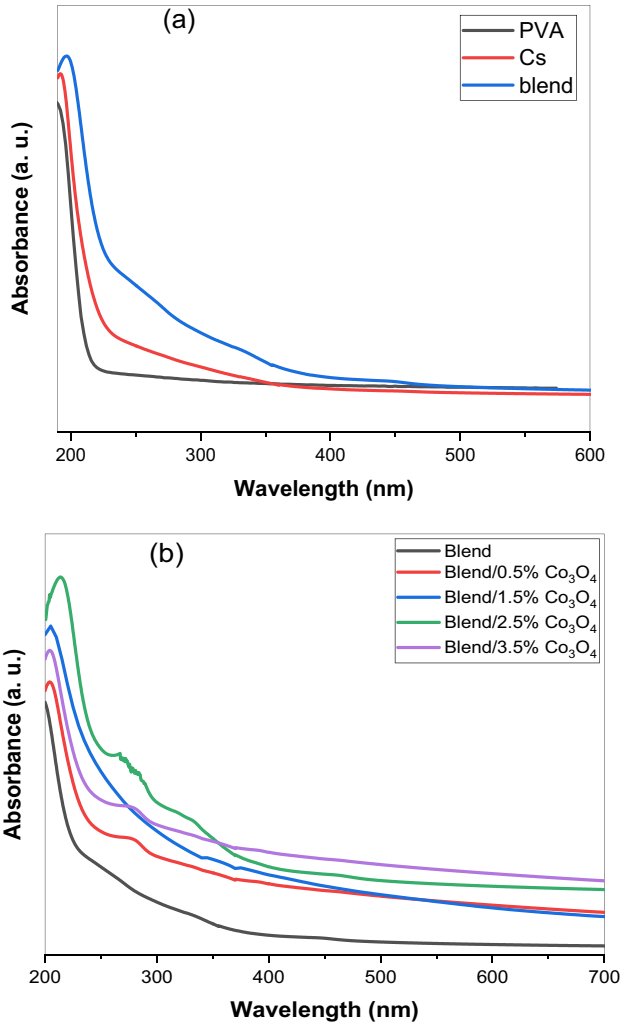

Fig. 4 UV–Vis absorption spectra of **a** pure PVA, Cs and PVA/Cs blend **b** pure blend and PVA/Cs/x(wt%) Co_3O_4 PNCs.

Thermal Analysis by TGA

TGA was utilized to examine the thermal stability of pure blend and Co_3O_4 NPs combined with PVA/Cs. TGA thermograms of pure blend and Co_3O_4NPs combined with PVA/Cs thin films are displayed in Fig. 6. Thermal degradation is observed in two steps in the TGA of pure blend and Co_3O_4/PVA/Cs PNCs. The first weight loss occurred between 25 °C and 113 °C, which is when the water and moisture that had been adsorbed evaporated. The main chain of the PVA/Cs matrix's breakdown, chemical stability, and intermolecular and intramolecular bonding are all related to the significant weight loss that was seen between 275 and 700 °C [52]. The two weight-loss stages of the pure blend are 113 °C and 275 °C. When Co_3O_4NPs are added to the PVA/Cs matrix, the weight loss of the nanocomposite films reduced. In the nanocomposits, the weight loss drops from 81% for the pure blend to 38% with the addition of 3.5%Co_3O_4 NPs. This

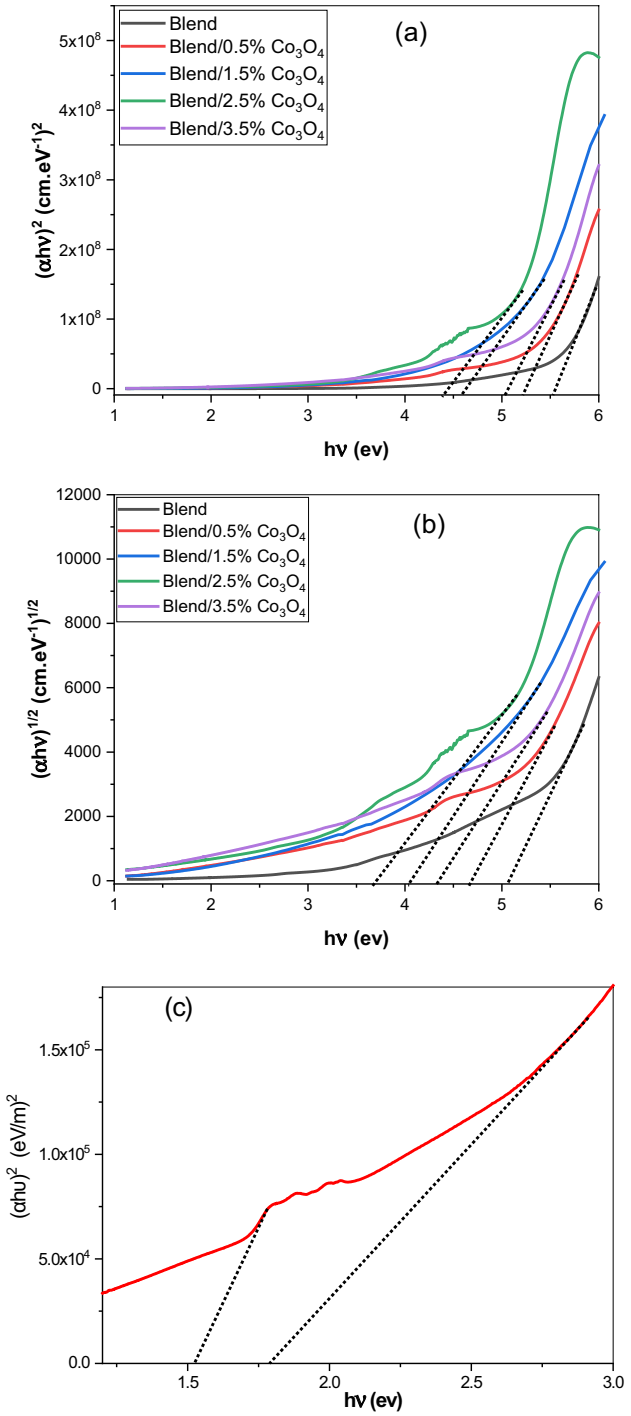

Fig. 5 The dependence of **a** $(\alpha h\nu)^2$, **b** $(\alpha h\nu)^{1/2}$ and **c** $(\alpha h\nu)^{1/2}$ on $h\nu$ for pure Co_3O_4 NPs and all the prepared films

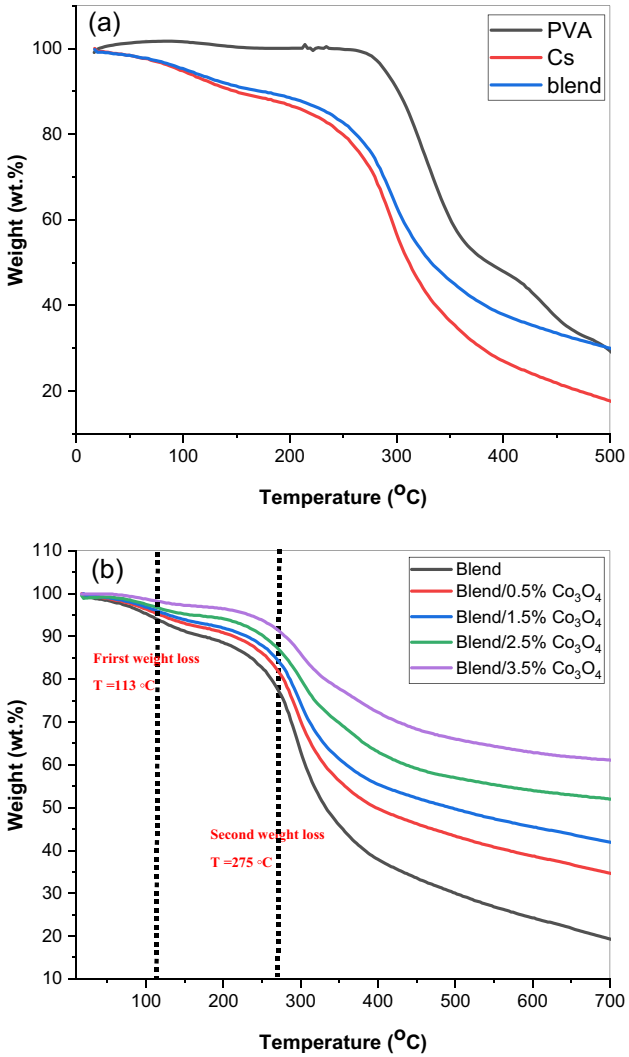

Fig. 6 The TGA thermograms of **a** pure PVA, Cs, and PVA/Cs blend **b** blend and blend doped with Co_3O_4 NPs

phenomenon may be explained by the polymer matrix's increased physicochemical bonding density. It depicts the physical binding density, which describes the quantity of non-electronic-sharing interactions between atoms, such as per unit volume, ionic-based interactions, as well as the chemical bonding density, which is the number of bonds, such as covalent and the weaker interactions involving electron-sharing, among the atoms of the PVA/Cs-Co_3O_4 nanocomposite per unit volume [53]. At 700 ◦C, no more weight loss was seen. As can be seen from the trend below, the PVA/Cs blend exhibits improved thermal stability as the concentration of Co_3O_4NPs increases while the percentage weight loss decreases. Furthermore, the TGA curves of the Co_3O_4/PVA/Cs nanocomposites shift toward higher temperatures as a result of the interaction between the blend and Co_3O_4NPs [54].

Mechanical Properties

The mechanical behavior of pristine blend and PVA/Cs-Co_3O_4 PNCs films was analyzed employing a Universal Testing Machine (UTM). Figure 7 illustrates the stress-strain

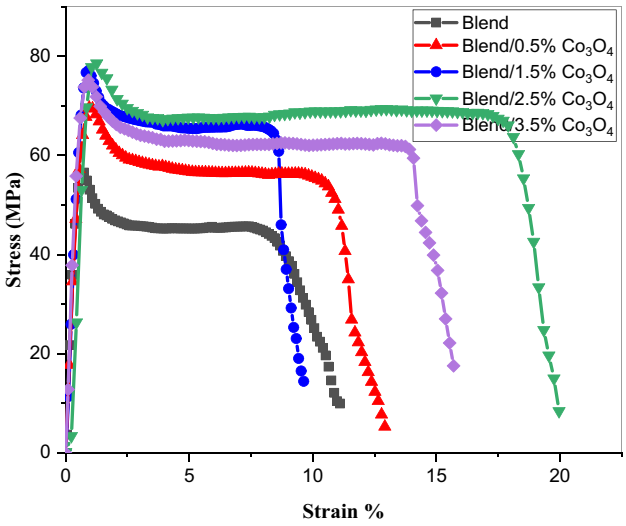

Fig. 7 Stress-strain curves of pure blend and PVA/Cs/x(wt%) Co_3O_4 PNCs films

curves for pristine blend and its corresponding PVA/Cs-Co_3O_4 PNCs. The curves reveal that the pure PVA/Cs film exhibits a lower stress-bearing capacity compared to the PVA/Cs-Co_3O_4 PNCs. The slope of the linear region of the stress-strain curves in Fig. 7 represents the Young's modulus of the respective samples. The mechanical properties of PVA/Cs-Co_3O_4 nanocomposites are exhibited in Table 1. Analysis of Young's modulus, tensile strength, and elongation% are essential to evaluate the suitability of material for food packaging applications. As seen from Table 1, tensile strength, Young's modulus, and elongation% of all PVA/Cs-Co_3O_4 nanocomposite films significantly surpass those of the pure blend. The PVA/Cs blend with 2.5 weight% Co_3O_4 exhibits the highest tensile strength of the composite. Strong interfacial adhesion between the blend chains and Co_3O_4 nanoparticles accounts for the enhanced tensile strength of the PVA/Cs-Co_3O_4 nanocomposite [55]. The composite's tensile strength also increases as the concentration of Co_3O_4 nanofiller increases up to 2.5 weight%. This suggests that the Co_3O_4 nanofiller has been dispersed more uniformly, creating a larger interfacial area and improving the blend's and Co_3O_4 interfacial adhesion [56]. The Young's modulus and tensile strength decrease when the concentration of Co_3O_4 NPs surpasses 2.5wt% because of the inadequate reinforcing effect of filler particles as a result of their aggregation. Poor polymer-filler interaction results from heterogeneous dispersion of aggregated NPs in the blend at higher loadings of Co_3O_4 nanoparticles [57]. The incorporation of 3.5% Co_3O_4-PVA/Cs resulted in a decrease in the toughness of the blend, which could be attributed to the increased rigidity and restricted molecular mobility caused by the strong interaction between Co_3O_4 nanofiller and blend [58]. Strong Co_3O_4 NP–PVA/Cs matrix interactions improve the material's Young's modulus and tensile strength, making it appropriate for food packaging [59].

Antimicrobial Properties

The antimicrobial efficacy of the pristine blend and Co_3O_4-PVA/Cs PNCs was assessed employing the disc diffusion method against a range of Gram-positive (*S. aureus*) and Gram-negative (*E. coli*) bacteria, as well as fungi (*C. albicans* and *A. niger*) as shown in Fig. 8. The effectiveness of the samples against microorganisms was assessed by measuring the inhibition zone diameters. The antibacterial activity of a commonly used standard antibiotic, ampicillin, and the antifungal drug, clotrimazole, was also evaluated. The tested PVA showed very little activity against microbial strains compared to chitosan, while chitosan showed properties slightly lower than those shown by pure blend. The Fig. 8 demonstrates that the PVA/Cs blend without Co_3O_4 nanoparticles exhibited limited antibacterial activity against both Gram-negative and Gram-positive bacterial strains. The addition of Co_3O_4 to the PVA/Cs blend demonstrated exceptional antibacterial efficacy against all bacteria tested. Additionally, the diameter of the clear zone grew with the increasing amount of Co_3O_4 in the polymer blend. For instance, the antibacterial activity against *S. aureus*, assessed by the inhibition zone diameter, demonstrated a positive correlation with the increasing content of Co_3O_4 NPs in the polymer blend. Similarly, a positive correlation between clear zone diameters and Co_3O_4 NPs content was observed for other tested bacteria. The polymer blend's antibacterial activity against *S. aureus*, *E. coli*, *C. albicans*, and *A. niger*

Table 1 The OBG (direct and indirect) values and mechanical properties for pure blend and Co_3O_4 doped PVA/Cs.

Samples	$E_{g\ indirect}$	$E_{g\ direct}$	Tensile Strength (MPa)	Toughness (MJ/m3)	Young's Modulus (MPa)	Elongation at Fracture%
PVA/Cs Blend	5.07	5.52	57.14	1.24	6.34	11.16
Blend/0.5%Co_3O_4	4.67	5.22	70.92	1.96	9.45	12.98
Blend/1.5% Co_3O_4	4.03	4.51	77.57	2.32	14.81	9.78
Blend/2.5% Co_3O_4	3.56	4.01	79.17	5.67	18.45	19.95
Blend/3.5% Co_3O_4	4.31	5.03	76.12	4.95	15.34	15.63

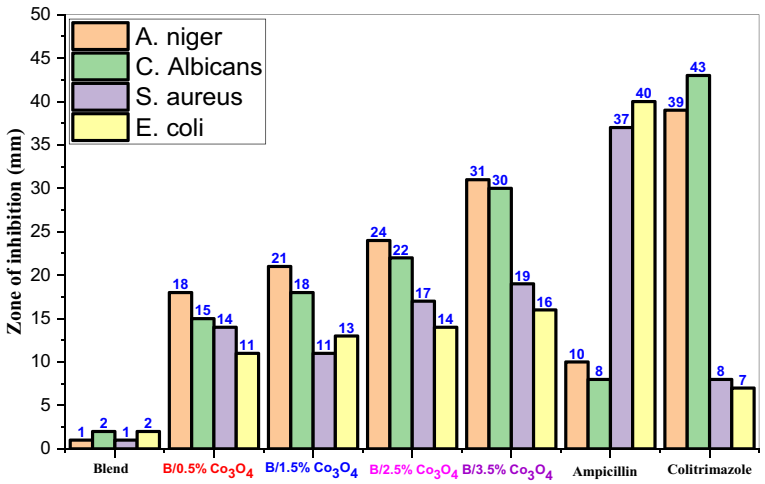

Fig. 8 Shows the antibacterial inhibition area diameter of Cs/PVA-Co_3O_4 PNCs films

increases when Co_3O_4 NPs are added. 3.5% Co_3O_4-PVA/Cs nanocomposite film exhibited the highest antibacterial activity against *A. niger*, with a zone of inhibition 31 mm. It is evident that when the concentration of Co_3O_4NPs rises, so does the zone of inhibition. The increased composition of Co_3O_4NPs in the 3.5% Co_3O_4-PVA/Cs nanocomposite may be the cause of the enhancement in its activity. Gram-positive *S. aureus* bacteria were more strongly inhibited by the Co_3O_4-PVA/Cs nanocomposite films than *E. coli* bacteria. This difference in the composition and structure of the bacteria's cell walls may be the cause of this. The microorganisms growth was effectively inhibited by the increase in weight of Co_3O_4NPs, the similar results were reported by Akhavan et al. [60]. There are potential differences in the observations that are reported, because the bacterial cell wall structure varies [1]. The Co_3O_4-PVA/Cs nanocomposites may specifically target the thick peptidoglycan layer of *E. coli*, increasing their antibacterial potential [61]. Several methods have been proposed to explain PVA/Cs-Co_3O_4's antibacterial activity, as illustrated in Fig. 9: (i) The polymer absorbs onto the target bacteria due to electrostatic attractions between its positively-charged chains and the negatively-charged bacterial cell walls, disrupting the cell wall [62]. (ii) Reactive oxygen species (ROS) production [63, 64]. (iii) One possible explanation for the inhibitory activity of nanoparticles could be their ability to enter microbes and

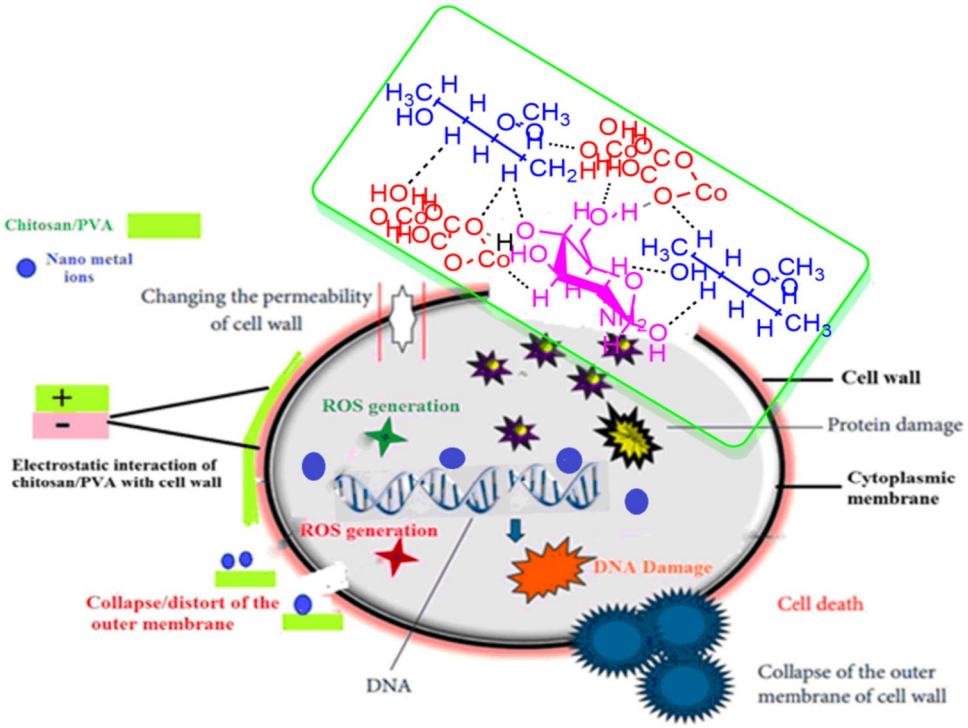

Fig. 9 Mechanism of antibacterial activity of Cs/PVA-Co_3O_4 nanocomposites

Table 2 lists earlier research on polymer nanocomposites and how they affected *S. aureus* and *E. coli*

Composition	E. coli (mm)	S. aureus (mm)	References
PVA/Chitosan/HAP/GO/Au	14.0	15.0	[67]
PVA/Spathodea campanulata/ZnO	2.4	3.0	[68]
PVDF/Cellulose acetate-TiO_2 PNCs	14.3	17.8	[69]
Cs/PEO/Ag/TiO_2	8.0	11.0	[70]
Co_3O_4/PANI PNCs	12.0	10.0	[71]
Co3O4/PPy PNCs	12.0	14.0	[72]
Polyketone/ZnO	3.0	11.0	[73]
Cs/PVA-3.5%Co_3O_4	16	19	The current work

cause harm through interactions with the phosphorus and sulfur groups found in DNA and proteins [65, 66]. Table 2 lists earlier research on polymer nanocomposites and how they affected *S. aureus* and *E. coli*. These findings suggest that nanocomposites' appropriate composition can be used to customize their potential antibacterial profile for use in food packaging applications.

Conclusions

Effective synthesis of Co_3O_4 nanoparticles using cobalt salt has been accomplished. The existence of Co_3O_4 NPs and the increased amorphous content of the polymer blend are validated by XRD analysis. The FTIR analysis confirms that the interactions between PVA/Cs blend functional groups and nanofiller. With the addition of nanoparticles, the intensity of the UV–visible absorption spectra increases. Because more energy states were introduced between the valence and conduction bands as the dopant concentration increased, the optical absorption edge and optical band gaps (both direct and indirect) showed a decreasing trend. The improved optical properties of the 2.5% Co_3O_4-PVA/Cs nanocomposite indicate that it may be a promising material for optoelectronic applications. The TGA analysis of PVA/Cs-Co_3O_4 nanocomposites revealed that the addition of Co_3O_4 nanoparticles enhanced the thermal stability of PVA/Cs. The Young's modulus, tensile strength, and elongation% of the blend were all improved by the Co_3O_4 nanoparticles, according to the results. Co_3O_4 nanoparticles integrated with PVA/Cs film demonstrated outstanding antibacterial activity against fungi (*A. niger* and *C. albicans*) as well as Gram-negative (*E. coli*) and Gram-positive (*S. aureus*) bacteria. Additionally, the Co_3O_4-PVA/Cs nanocomposite's potential antibacterial profile can be tailored for food packaging and biomedical applications with the help of an appropriate composition.

Author Contributions HA: Supervision, conceptualization, methodology, Writing—original draft, Writing—review & editing. AMA: Visualization, software, Writing—review & editing. NYE: Visualization, investigation, data curation, Writing—review & editing. AR: Data curation, Writing—review & editing, visualization, software.

Funding This work was supported and funded by the Deanship of Scientific Research at Imam Mohammad Ibn Saud Islamic University (IMSIU) (Grant number IMSIU RG23032).

Data Availability No datasets were generated or analysed during the current study.

Declarations

Declaration of Competing Interest The authors declare that they have no known competing financial interests or personal relationships that could have appeared to influence the work reported in this paper.

References

1. Shubha A, Manohara SR, Siddlingeshwar B, Daima HK, Singh M, Revaprasadu N (2022) Ternary poly(2-ethyl-2-oxazoline)-polyvinylpyrrolidone-graphene nanocomposites: Thermal, electrical, dielectric, mechanical, and antibacterial profiling. Diam Relat Mater 125:109001. https://doi.org/10.1016/J.DIAMOND.2022.109001
2. Albalawi H, Alharbi EM, Al-Sulami AI, Al-Qahtani N, Farea MO, Rajeh A (2023) Synthesis and characterization of sodium alginate/polyvinyl alcohol/zinc oxide/iron oxide nanocomposites for electrochemical applications. Polym Compos 44:1762–1771. https://doi.org/10.1002/pc.27203
3. Alzahrani HS, Al-Sulami AI, Alsulami QA, Rajeh A (2022) A systematic study of structural, conductivity, linear, and nonlinear optical properties of PEO/PVA-MWCNTs/ZnO nanocomposites films for optoelectronic applications. Opt Mater (Amst) 133:112900. https://doi.org/10.1016/J.OPTMAT.2022.112900
4. Govindasamy GA, Mydin RBSMN, N.F.W W, Sreekantan S (2022) Novel dual-ionic ZnO/CuO embedded in porous chitosan biopolymer for wound dressing application: Physicochemical, bactericidal, cytocompatibility and wound healing profiles. Mater Today Commun 33:104545. https://doi.org/10.1016/J.MTCOMM.2022.104545
5. Abutalib MM, Rajeh A (2020) Structural, thermal, optical and conductivity studies of Co/ZnO nanoparticles doped CMC Polymer for solid state battery applications. Polym Test 91:106803. https://doi.org/10.1016/J.POLYMERTESTING.2020.106803
6. Bharati DC, Rawat P, Saroj AL (2021) Structural, thermal, and ion dynamics studies of PVA-CS-NaI-based biopolymer electrolyte

films. J Solid State Electrochem 25:1727–1741. https://doi.org/10.1007/s10008-021-04946-6
7. Govindasamy GA, Mydin RBSMN, Gadaime NKR, Sreekantan S (2023) Phytochemicals, Biodegradation, Cytocompatibility and Wound Healing profiles of Chitosan Film embedded Green Synthesized Antibacterial ZnO/CuO Nanocomposite. J Polym Environ 31:4393–4409. https://doi.org/10.1007/s10924-023-02902-1
8. Saroj AL, Krishnamoorthi S, Singh RK (2017) Structural, thermal and electrical transport behaviour of polymer electrolytes based on PVA and imidazolium based ionic liquid. J Non Cryst Solids 473:87–95. https://doi.org/10.1016/J.JNONCRYSOL.2017.07.035
9. Varshney PK, Gupta S (2011) Natural polymer-based electrolytes for electrochemical devices: a review. Ionics (Kiel) 17:479–483. https://doi.org/10.1007/s11581-011-0563-1
10. Agrawal P, Strijkers GJ, Nicolay K (2010) Chitosan-based systems for molecular imaging. Adv Drug Deliv Rev 62:42–58. https://doi.org/10.1016/J.ADDR.2009.09.007
11. Leones R, Sabadini RC, Esperança JMSS, Pawlicka A, Silva MM (2017) Effect of storage time on the ionic conductivity of chitosan-solid polymer electrolytes incorporating cyano-based ionic liquids. Electrochim Acta 232:22–29. https://doi.org/10.1016/J.ELECTACTA.2017.02.053
12. Saroj AL, Singh RK (2012) Thermal, dielectric and conductivity studies on PVA/Ionic liquid [EMIM][EtSO4] based Polymer electrolytes. J Phys Chem Solids 73:162–168. https://doi.org/10.1016/J.JPCS.2011.11.012
13. Mobarak NN, Ahmad A, Abdullah MP, Ramli N, Rahman MYA (2013) Conductivity enhancement via chemical modification of chitosan based green polymer electrolyte. Electrochim Acta 92:161–167. https://doi.org/10.1016/J.ELECTACTA.2012.12.126
14. Hezma AM, Rajeh A, Mannaa MA (2019) An insight into the effect of zinc oxide nanoparticles on the structural, thermal, mechanical properties and antimicrobial activity of Cs/PVA composite, colloids surfaces a physicochem. Eng Asp 581:123821. https://doi.org/10.1016/J.COLSURFA.2019.123821
15. Guo S, Dong S, Wang E (2010) Three-dimensional Pt-on-Pd bimetallic nanodendrites supported on Graphene Nanosheet: facile synthesis and used as an advanced nanoelectrocatalyst for methanol oxidation. ACS Nano 4:547–555. https://doi.org/10.1021/nn9014483
16. Lakshmanan A, Surendran P, Sakthy Priya S, Balakrishnan K, Geetha P, Rameshkumar P, Hegde TA, Vinitha G, Kannan K (2020) Investigations on structural, optical, dielectric, electronic polarizability, Z-scan and antibacterial properties of Ni/Zn/Fe2O4 nanoparticles fabricated by microwave-assisted combustion method. J Photochem Photobiol A Chem 402:112794. https://doi.org/10.1016/J.JPHOTOCHEM.2020.112794
17. Nachimuthu S, Thangavel S, Kannan K, Selvakumar V, Muthusamy K, Raza Siddiqui M, Mohammad Wabaidur S, Parvathiraja C (2022) Lawsonia inermis mediated synthesis of ZnO/Fe2O3 nanorods for photocatalysis – biological treatment for the enhanced effluent treatment, antibacterial and antioxidant activities. Chem Phys Lett 804:139907. https://doi.org/10.1016/J.CPLETT.2022.139907
18. Li Y, Zhao J, Dan Y, Ma D, Zhao Y, Hou S, Lin H, Wang Z (2011) Low temperature aqueous synthesis of highly dispersed Co3O4 nanocubes and their electrocatalytic activity studies. Chem Eng J 166:428–434. https://doi.org/10.1016/J.CEJ.2010.10.080
19. Warang T, Patel N, Santini A, Bazzanella N, Kale A, Miotello A (2012) Pulsed laser deposition of Co3O4 nanoparticles assembled coating: role of substrate temperature to tailor disordered to crystalline phase and related photocatalytic activity in degradation of methylene blue. Appl Catal A Gen 423–424. https://doi.org/10.1016/J.APCATA.2012.02.037
20. Bhushan M, Kumar Y, Periyasamy L, Viswanath AK (2018) Antibacterial applications of α-Fe2O3/Co3O4 nanocomposites and study of their structural, optical, magnetic and cytotoxic characteristics. Appl Nanosci 8:137–153. https://doi.org/10.1007/s13204-018-0656-5
21. Gupta V, Kant V, Sharma AK, Sharma M (2022) Comparative evaluation of antibacterial potentials of nano cobalt oxide with standard antimicrobials. J Indian Chem Soc 99:100533. https://doi.org/10.1016/J.JICS.2022.100533
22. Abdel-Wareth MTA, El-Hagrassi AM, Abdel-Aziz MS, Nasr SM, Ghareeb MA (2019) Biological activities of endozoic fungi isolated from *Biomphalaria alexandrina* snails maintained in different environmental conditions. Int J Environ Stud 76:780–799. https://doi.org/10.1080/00207233.2019.1620535
23. Letsholathebe D, Thema FT, Mphale K, Mohamed HEA, Holonga KJ, Ketlhwaafetse R, Chimidza S (2021) Optical and structural stability of Co3O4 nanoparticles for photocatalytic applications, Mater. Today Proc. 36 499–503. https://doi.org/10.1016/J.MATPR.2020.05.205
24. Lakra R, Kumar R, Nath Thatoi D, Kumar Sahoo P (2021) Synthesis and characterization of cobalt oxide (Co3O4) nanoparticles. Mater Today Proc 41:269–271. https://doi.org/10.1016/J.MATPR.2020.09.099
25. Murugesan R, Sivakumar S, Karthik K, Anandan P, Haris M (2019) Structural, optical and magnetic behaviors of Fe/Mn-doped and co-doped CdS thin films prepared by spray pyrolysis method. Appl Phys A 125:281. https://doi.org/10.1007/s00339-019-2577-x
26. Karthik K, Pushpa S, Madhukara Naik M, Vinuth M (2020) Influence of Sn and Mn on structural, optical and magnetic properties of spray pyrolysed CdS thin films. Mater Res Innov 24:82–86. https://doi.org/10.1080/14328917.2019.1597436
27. Abdullah OG, Hanna RR, Salman YAK, Aziz SB (2018) Characterization of Lithium Ion-conducting blend Biopolymer Electrolyte based on CH–MC Doped with LiBF4. J Inorg Organomet Polym Mater 28:1432–1438. https://doi.org/10.1007/s10904-018-0802-2
28. Hasegawa M, Isogai A, Onabe F, Usuda M, Atalla RH (1992) Characterization of cellulose–chitosan blend films. J Appl Polym Sci 45:1873–1879. https://doi.org/10.1002/app.1992.070451101
29. Ebtesam M, Alharbi, Rajeh A (2022) Tailoring the structural, optical, dielectric, and electrical properties of PEO/PVA blend using graphene nanoplates for energy storage devices. J Mater Sci: Mater Electron 33(28):22196–22207
30. Shukur MF, Kadir MFZ (2015) Hydrogen ion conducting starch-chitosan blend based electrolyte for application in electrochemical devices. Electrochim Acta 158:152–165. https://doi.org/10.1016/J.ELECTACTA.2015.01.167
31. Letsholathebe D et al (2021) Optical and structural stability of Co3O4 nanoparticles for photocatalytic applications. Materials Today: Proceedings 36 : 499–503
32. Hoang T, Ramadass K, Loc TT, Mai TT, Giang LD, Thang VV, Tuan TM, Chinh NT (2019) Novel Drug Delivery System based on Ginsenoside Rb1 loaded to Chitosan/Alginate Nanocomposite Films. J Nanosci Nanotechnol 19:3293–3300. https://doi.org/10.1166/jnn.2019.16116
33. Abou El-Reash YG, Abdelghany AM, Elrazak AA (2016) Removal and separation of Cu(II) from aqueous solutions using nano-silver chitosan/polyacrylamide membranes. Int J Biol Macromol 86:789–798. https://doi.org/10.1016/j.ijbiomac.2016.01.101
34. Zhu J, Li Q, Che Y, Liu X, Dong C, Chen X, Wang C (2020) Effect of Na2CO3 on the microstructure and Macroscopic Properties and mechanism analysis of PVA/CMC Composite Film. Polym (Basel) 12:453. https://doi.org/10.3390/polym12020453
35. Mansur HS, Sadahira CM, Souza AN, Mansur AAP (2008) FTIR spectroscopy characterization of poly (vinyl alcohol) hydrogel with different hydrolysis degree and chemically crosslinked with

glutaraldehyde. Mater Sci Eng C 28:539–548. https://doi.org/10.1016/J.MSEC.2007.10.088
36. Lewandowska K (2015) Miscibility and physical properties of chitosan and polyacrylamide blends. J Mol Liq 209:301–305. https://doi.org/10.1016/J.MOLLIQ.2015.05.049
37. Rani P, Deshmukh K, Kadlec J, Krishna Karthik TV, Khadheer SK, Pasha (2023) Dielectric properties of graphene/nano-Fe2O3 filled poly (vinyl alcohol)/Chitosan blends. Mater Chem Phys 295:126986. https://doi.org/10.1016/J.MATCHEMPHYS.2022.126986
38. Ali H, Tiama TM, Ismail AM (2021) New and efficient NiO/chitosan/polyvinyl alcohol nanocomposites as antibacterial and dye adsorptive films. Int J Biol Macromol 186:278–288. https://doi.org/10.1016/J.IJBIOMAC.2021.07.055
39. Sadiq NM, Aziz SB, Kadir MFZ, Development of Flexible Plasticized Ion Conducting Polymer Blend Electrolytes Based on Polyvinyl Alcohol (PVA) (2022) Chitosan (CS) with high Ion Transport parameters Close to Gel based electrolytes. Gels 8:153. https://doi.org/10.3390/gels8030153
40. Govindasamy GA, Mydin RBSMN, Sreekantan S, Harun NH (2021) Compositions and antimicrobial properties of binary ZnO–CuO nanocomposites encapsulated calcium and carbon from Calotropis gigantea targeted for skin pathogens. Sci Rep 11:99. https://doi.org/10.1038/s41598-020-79547-w
41. Alsulami QA, Rajeh A (2023) Modification and development in the microstructure of PVA/CMC-GO/Fe3O4 nanocomposites films as an application in energy storage devices and magnetic electronics industry. Ceram Int 49:14399–14407. https://doi.org/10.1016/J.CERAMINT.2023.01.029
42. Suvarna S, Furhan MT, Ramesan (2022) Optical and electrical properties of copper alumina nanoparticles reinforced chlorinated polyethylene composites for optoelectronic devices. J Indian Chem Soc 99:100772. https://doi.org/10.1016/J.JICS.2022.100772
43. Ali FM, Kershi RM, Sayed MA, AbouDeif YM (2018) Evaluation of structural and optical properties of Ce3 + ions doped (PVA/PVP) composite films for new organic semiconductors. Phys B Condens Matter 538:160–166. https://doi.org/10.1016/J.PHYSB.2018.03.031
44. Sengwa RJ, Dhatarwal P, Choudhary S (2020) A comparative study of different metal oxide nanoparticles dispersed PVDF/PEO blend matrix-based advanced multifunctional nanodielectrics for flexible electronic devices. Mater Today Commun 25:101380. https://doi.org/10.1016/J.MTCOMM.2020.101380
45. Charan CP, Sengwa RJ, Saraswat M (2024) Synergistic effect of polymer blend compositions on the structural, thermal, optical, and broadband dielectric properties of P(VDF-HFP)/PEO/ZnO polymer nanocomposites. Chem Phys Impact 8:100410. https://doi.org/10.1016/J.CHPHI.2023.100410
46. Morsi MA, Rajeh A, Al-Muntaser AA (2019) Reinforcement of the optical, thermal and electrical properties of PEO based on MWCNTs/Au hybrid fillers: nanodielectric materials for organo-electronic devices. Compos Part B Eng 173:106957. https://doi.org/10.1016/J.COMPOSITESB.2019.106957
47. Alsulami QA, Rajeh A (2021) Synthesis of the SWCNTs/TiO2 nanostructure and its effect study on the thermal, optical, and conductivity properties of the CMC/PEO blend. Results Phys 28:104675. https://doi.org/10.1016/J.RINP.2021.104675
48. Soliman TS, Zaki MF, Hessien MM, Elkalashy SI (2021) The structure and optical properties of PVA-BaTiO3 nanocomposite films. Opt Mater (Amst) 111:110648. https://doi.org/10.1016/J.OPTMAT.2020.110648
49. Keshtov ML, Konstantinov IO, Khokhlov AR, Kuklin SA, Alekseev VG, Ostapov IE, Zou Y, Singhal R, Dahiya H, Sharma GD (2022) New wide band gap π-conjugated copolymers based on anthra[1,2-b: 4,3-b': 6,7-c''] trithiophene-8,12-dione for high performance non-fullerene polymer solar cells with an efficiency of 15.07%. Polym (Guildf) 251:124892. https://doi.org/10.1016/J.POLYMER.2022.124892
50. Deori K, Ujjain SK, Sharma RK, Deka S (2013) Morphology Controlled Synthesis of Nanoporous Co_3O_4 Nanostructures and their charge storage characteristics in Supercapacitors. ACS Appl Mater Interfaces 5:10665–10672. https://doi.org/10.1021/am4027482
51. Ali GAM, Fouad OA, Makhlouf SA (2013) Structural, optical and electrical properties of sol–gel prepared mesoporous Co3O4/SiO2 nanocomposites. J Alloys Compd 579:606–611. https://doi.org/10.1016/J.JALLCOM.2013.07.095
52. Alghamdi HM, Rajeh A (2022) Synthesis of CoFe2O4/MWCNTs nanohybrid and its effect on the optical, thermal, and conductivity of PVA/CMC composite as an application in electrochemical devices. J Inorg Organomet Polym Mater 32(5):1935–1949
53. Rajeh A et al (2023) Alteration in the Structural, Optical, Thermal, Electrical, and Dielectric properties of PMMA/PVDF blend by Incorporation of Ni/ZnO Nanohybrid for Optoelectronic and Energy Storage Devices. J Inorg Organomet Polym Mater : 1–11
54. Alghamdi HM, Rajeh A (2023) Study of the photoluminescence, optical, thermal, and electrical parameters of the Cs/PVP blend/zinc oxide nanorods films for energy storage devices. Polym Test 124:108093. https://doi.org/10.1016/J.POLYMERTESTING.2023.108093
55. Ramesan MT, Jayakrishnan P, Anilkumar T, Mathew G (2018) Influence of copper sulphide nanoparticles on the structural, mechanical and dielectric properties of poly(vinyl alcohol)/poly(vinyl pyrrolidone) blend nanocomposites. J Mater Sci Mater Electron 29:1992–2000. https://doi.org/10.1007/s10854-017-8110-0
56. Thakur AK (2011) Mechanism for improvement in mechanical and thermal stability in dispersed phase polymer composites. Ionics (Kiel) 17:109–120. https://doi.org/10.1007/s11581-010-0498-y
57. Ramesan MT, Sampreeth T (2017) Synthesis, characterization, material properties and sensor application study of polyaniline/niobium doped titanium dioxide nanocomposites. J Mater Sci Mater Electron 28:16181–16191. https://doi.org/10.1007/s10854-017-7519-9
58. Raheel M, Yao K, Gong J, Chen X, Liu D, Lin Y, Cui D, Siddiq M, Tang T (2015) Poly(vinyl alcohol)/GO-MMT nanocomposites: Preparation, structure and properties. Chin J Polym Sci 33:329–338. https://doi.org/10.1007/s10118-015-1586-2
59. Mathew S, Mathew J, Radhakrishnan EK (2019) Polyvinyl alcohol/silver nanocomposite films fabricated under the influence of solar radiation as effective antimicrobial food packaging material. J Polym Res 26:223. https://doi.org/10.1007/s10965-019-1888-0
60. Akhavan A, Khoylou F, Ataeivarjovi E (2017) Preparation and characterization of gamma irradiated Starch/PVA/ZnO nanocomposite films. Radiat Phys Chem 138:49–53. https://doi.org/10.1016/J.RADPHYSCHEM.2017.02.057
61. Mohammed H, Kumar A, Bekyarova E, Al-Hadeethi Y, Zhang X, Chen M, Ansari MS, Cochis A, Rimondini L (2020) Antimicrobial mechanisms and effectiveness of Graphene and Graphene-Functionalized Biomaterials. A scope review, front. Bioeng Biotechnol 8:498689. https://doi.org/10.3389/fbioe.2020.00465
62. Kannan K, Radhika D, Gnanasangeetha D, Krishna LS, Gurushankar K (2021) Y3 + and Sm3 + co-doped mixed metal oxide nanocomposite: structural, electrochemical, photocatalytic, and antibacterial properties. Appl Surf Sci Adv 4:100085. https://doi.org/10.1016/J.APSADV.2021.100085
63. Diez-Pascual AM (2017) Development and characterization of chitosan-grafted polycaprolactone / poly (3-hydroxybutyrate-CO-3-hydroxyhexanoate) fiber blends for tissue engineering applications. Int J Comput Methods Exp Meas 5:713–722. https://doi.org/10.2495/CMEM-V5-N5-713-722

64. Rangayasami A, Kannan K, Joshi S, Subban M (2020) Bioengineered silver nanoparticles using Elytraria Acaulis (L.f.) Lindau leaf extract and its biological applications. Biocatal Agric Biotechnol 27:101690. https://doi.org/10.1016/J.BCAB.2020.101690
65. Kannan K, Radhika D, Kasai RD, Gnanasangeetha D, Palani G, Gurushankar K, Koutavarapu R, Lee D-Y, Shim J (2022) Facile fabrication of novel ceria-based nanocomposite (CYO-CSO) via co-precipitation: Electrochemical, photocatalytic and antibacterial performances. J Mol Struct 1256:132519. https://doi.org/10.1016/J.MOLSTRUC.2022.132519
66. Chinnaiah K, Krishnamoorthi R, Kannan K, Sivaganesh D, Saravanakumar S, Theivasanthi T, Palko N, Grishina M, Maik V, Gurushankar K (2022) Ag nanoparticles synthesized by Datura metel L. Leaf extract and their charge density distribution, electrochemical and biological performance. Chem Phys Lett 807:140083. https://doi.org/10.1016/J.CPLETT.2022.140083
67. Yahia IS, Shkir M, Keshk SMAS (2020) Physicochemical properties of a nanocomposite (graphene oxide-hydroxyapatite-cellulose) immobilized by Ag nanoparticles for biomedical applications. Results Phys 16:102990. https://doi.org/10.1016/J.RINP.2020.102990
68. Goudar N, Vanjeri VN, Kasai D, Gouripur G, Malabadi RB, Masti SP, Chougale RB (2021) ZnO NPs Doped PVA/Spathodea campanulata Thin films for Food Packaging. J Polym Environ 29:2797–2812. https://doi.org/10.1007/s10924-021-02070-0
69. Senthil Muthu Kumar T, Senthilkumar K, Ratanit M, Rajini N, Chanunpanich N, Hariram N, Pornwongthong P, Siengchin S (2021) Influence of Titanium Dioxide particles on the filtration of 1,4-Dioxane and Antibacterial Properties of Electrospun Cellulose Acetate and polyvinylidene fluoride nanofibrous membranes. J Polym Environ 29:775–784. https://doi.org/10.1007/s10924-020-01919-0
70. Abutalib MM, Rajeh A (2021) Enhanced structural, electrical, mechanical properties and antibacterial activity of Cs/PEO doped mixed nanoparticles (Ag/TiO2) for food packaging applications. Polym Test 93:107013. https://doi.org/10.1016/J.POLYMERTESTING.2020.107013
71. Kumar H, Luthra M, Punia M, Singh RM (2021) Co3O4/PANI nanocomposites as a photocatalytic, antibacterial and anticorrosive agent: experimental and theoretical approach. Colloid Interface Sci Commun 45:100512. https://doi.org/10.1016/J.COLCOM.2021.100512
72. Kumar H, Luthra M, Punia M, Kaur P, Kumar R (2023) Co_3O_4 quantum dot decorated polypyrrole nanocomposites as a flexible, conducting, anticorrosive and antibacterial agent: sustainable experimental and theoretical approach. RSC Sustain 1:523–534. https://doi.org/10.1039/D2SU00104G
73. Alamry KA, Almehmadi SJ, Elfaky MA, Al-Shareef HF, Hussein SJAMA (2020) Enhanced antimicrobial activity of new arylidene-based polyketone nanocomposite materials. Polym Technol Mater 59:1973–1986